X-ray Absorption Study of the Solvation Structure of Cu²⁺ in Methanol and Dimethyl Sulfoxide

Andrea Zitolo,*,[†] Giovanni Chillemi,[‡] and Paola D'Angelo*,[†]

[†]Dipartimento di Chimica, Università di Roma "La Sapienza", Piazzale A. Moro 5, 00185 Roma, Italy

[‡]CASPUR, Inter-University Consortium for Supercomputing in Research, via dei Tizii 6b, 00185 Roma, Italy

S *Supporting Information*

ABSTRACT: The solvation structure of Cu²⁺ in methanol (MeOH) and dimethyl sulfoxide (DMSO) has been determined by studying both the extended X-ray absorption fine structure (EXAFS) and the X-ray absorption near-edge structure (XANES) regions of the K-edge absorption spectra. The EXAFS technique has been found to provide a very accurate determination of the next-neighbor coordination distances, but it is inconclusive in the determination of the coordination numbers and polyhedral environment. Conversely, quantitative analysis of the XANES spectra unambiguously shows the presence of an average 5-fold coordination in both the MeOH and DMSO solution, ruling out the usually proposed octahedral Jahn−Teller distorted geometry. The EXAFS and XANES techniques provide coherent values of the Cu−O first-shell distances that are coincident in the two solvents. This investigation shows that the combined analysis of the EXAFS and XANES data allows a reliable determination of the structural properties of electrolyte solutions, which is very difficult to achieve with other experimental techniques.
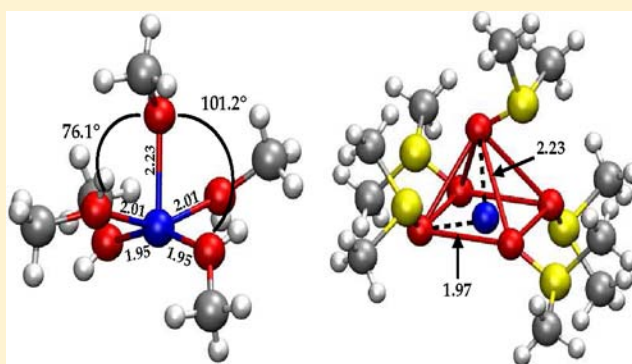
1. INTRODUCTION

Understanding the solvation structure around a metal ion is a first important step to understanding many physical and chemical properties of the metal ion in solution. After iron and zinc, copper is the third most abundant metal in the human body, and because of its biological importance, a large number of structural studies have been carried out, mainly in aqueous solution. For the last 40 years, the aqueous chemistry of copper was dominated by the $[Cu(OH_2)_6]^{2+}$ complex, represented as a Jahn−Teller (JT) distorted octahedron, because of its electronic d^9 configuration.[1] However, more recently the results obtained from a large variety of techniques, such as extended X-ray absorption fine structure (EXAFS), X-ray absorption near-edge structure (XANES), neutron diffraction, and molecular dynamic, indicate the existence of a 5-fold coordination.[2−9]

The solvation structure of the Cu²⁺ ion has also been studied in some nonaqueous solvents in order to understand how the nature and bulkiness of the ligands govern the coordination geometry around the metal ion.[10−13] In the case of complex formation between Cu²⁺ and some oxygen-donating solvent, such as methanol (MeOH) and dimethyl sulfoxide (DMSO), all of the previous studies suggest a distorted octahedral solvation structure, due to the JT effect.[13−15] However, validation of this model suffers from experimental difficulties in the determination of the structural parameters of the axial sites.[16−19] The EXAFS equatorial Cu−O bond lengths provide a distance value of 1.97 Å in a MeOH solution[13] and values in the 1.96−1.98 Å range in a DMSO solution,[13,14] but in both

cases, no detailed information on the axial Cu−O bond distances is given. Because an accurate determination of the solvation geometry of Cu²⁺ in liquid MeOH and DMSO is still lacking, we decided to apply a short-range-order technique such as X-ray absorption spectroscopy (XAS), which has proven to be a valuable tool to determine the local environment around a specific atom in a large variety of solutions.[20−31] EXAFS is a well-known method to obtain accurate structural information on metal sites, but this technique is not very sensitive to the number of ligands and to their chemical nature.[22,25,32]

Conversely, XANES can provide useful three-dimensional information because of the higher sensitivity of the low-energy region of the absorption spectrum to the geometrical arrangement of the atoms around the photoabsorber. Because of recent theoretical advances, it is now possible to apply the fitting procedures generally employed to interpret the EXAFS data[33,34] also to the XANES region,[35−37] so that the whole energy range of the absorption spectrum can be used for a quantitative determination of the structural parameters.

In this work, we present a combined EXAFS and XANES analysis of Cu²⁺ in MeOH and DMSO solutions to provide a definitive answer to the ion coordination geometry in these systems.

2. MATERIALS AND METHODS

2.1. XAS Measurements. 0.1 M solutions of Cu^{2+} in MeOH and DMSO were prepared by dissolving appropriate amounts of $Cu(CF_3SO_3)_2$ in MeOH (Aldrich) and in DMSO (Aldrich) freshly distilled over calcium hydride (Fluka) under reduced pressure. Cu K-edge XAS spectra were obtained using the EMBL spectrometer at DESY.[38] Spectra were recorded at room temperature in transmission mode using a Si(111) double-crystal monochromator detuned to 30% for harmonic rejection.[39] Data points were collected for 1 s each, and three spectra were recorded and averaged after an absolute energy calibration was performed.[39] The edge position did not move during the data collection, showing that no photoreduction of the Cu^{2+} ion took place. The DORIS III storage ring was running at an energy of 4.4 GeV with positron currents between 120 and 90 mA. The solutions were kept in a cell with Kapton film windows and a Teflon spacer of 2 mm.

2.2. EXAFS Data Analysis. The EXAFS data analysis was performed with the GNXAS code using previously developed and widely applied methods.[33,34] In the GNXAS approach, interpretation of the experimental data is based on decomposition of the EXAFS $\chi(k)$ signal (defined as the oscillation with respect to the atomic background cross section normalized to the corresponding K-edge channel cross section) into a summation over n-body distribution functions $\gamma^{(n)}$ calculated by means of the multiple-scattering (MS) theory. Each signal has been calculated in the muffin-tin (MT) approximation using the Hedin−Lundqvist (HL) energy-dependent exchange and correlation potential model, which includes inelastic loss effects.

Several EXAFS investigations on electrolyte solutions have shown that a correct description of the first solvation sphere has to account for asymmetry in the distribution of the ion−solvent distances.[21−26,28−31] Therefore, the Cu−O first coordination shells have been modeled with Γ-like distribution functions, which depend on four parameters, namely, the coordination number N, the average distance R, the mean-square variation σ^2, and the skewness β. Note that β is related to the third cumulant C_3 through the relation $C_3 = \sigma^3\beta$.

Both the MeOH and DMSO spectra have been calculated using four solvent molecules in the equatorial plane and either one or two solvent ligands in the axial positions. The total $\chi(k)$ signals were calculated including the Cu−O and Cu−H two-body signals associated with the solvent molecules in the first shell for MeOH, while only the Cu−O two-body signal was included for DMSO. XAS is endowed with the unique capability of providing quantitative information on the three-body distribution functions in disordered systems. The γ^3 signal associated with the O−Cu−O angle of the equatorial plane has been included in the analyses. Moreover, the MS signals associated with the Cu−O−C and Cu−O−S three-body distributions have been considered for MeOH and DMSO, respectively. In this case, the only structural parameters are the Cu−O and O−C bond distances and the Cu−O−C bond angle for MeOH and the Cu−O and O−S bond distances and the Cu−O−S bond angle for DMSO. The Cu···C and Cu···S two-body signals are calculated starting from the same structural parameters.

Least-squares fits of the EXAFS raw experimental data have been performed by minimizing a residual function of the type

$$R_i(\{\lambda\}) = \sum_{i=1}^{N} \frac{[\alpha_{\text{exp}}(E_i) - \alpha_{\text{mod}}(E_i; \lambda_1, \lambda_2, ..., \lambda_p)]^2}{\sigma_i^2} \quad (1)$$

where N is the number of experimental points E_i, $\{\lambda\} = (\lambda_1, \lambda_2, ..., \lambda_p)$ are the p parameters to be refined, and σ_i^2 is the noise variance associated with each experimental point $\alpha_{\text{exp}}(E_i)$. The standard deviations given for the refined parameters in Table 1 are obtained from k^2-weighted least-squares refinements of the EXAFS function $\chi(k)$ and do not include systematic errors of the measurements. Additional nonstructural parameters were minimized, namely, E_0 (core ionization threshold energy) and S_0^2.

2.3. XANES Data Analysis. The XANES data analysis has been carried out with the MXAN[35−37] code in the framework of the full MS

Table 1. Best-Fit Parameters Obtained from Analysis of the EXAFS Spectra of Cu^{2+} in MeOH and DMSO[a]

	N_c	R (Å)	σ^2 (Å²)	β
		Cu^{2+} in MeOH		
5-fold coordination				
Cu−O$_{eq}$	4	1.96(1)	0.005(1)	0.0(1)
Cu−O$_{ax}$	1	2.28(2)	0.010(3)	0.5(1)
6-fold coordination				
Cu−O$_{eq}$	4	1.96(1)	0.005(1)	0.0(1)
Cu−O$_{ax}$	2	2.32(2)	0.023(3)	0.8(1)
		Cu^{2+} in DMSO		
5-fold coordination				
Cu−O$_{eq}$	4	1.95(1)	0.005(1)	0.0 (1)
Cu−O$_{ax}$	1	2.29(2)	0.012(3)	0.5(1)
6-fold coordination				
Cu−O$_{eq}$	4	1.95(1)	0.005(1)	0.0(1)
Cu−O$_{ax}$	2	2.33(2)	0.025(3)	0.8(1)

[a]N_c is the coordination number, R is the interatomic distance, σ^2 is the DW factor, and β is the asymmetry parameter.

scheme. The MXAN method is based on the MT approximation for the shape of the potential and uses a complex optical potential, based on the local density approximation of the self-energy of the excited photoelectron. The self-energy is calculated in the framework of the HL scheme. To avoid the relevant overdamping at low energies, MXAN uses a phenomenological approach to calculate the inelastic losses on the basis of a convolution of the theoretical spectrum. This calculation uses only the real part of the HL potential, with a suitable Lorentzian function having an energy-dependent width of the form $\Gamma_{\text{tot}}(E) = \Gamma_c + \Gamma_{\text{mfp}}(E)$. The constant part, Γ_c, includes the core hole lifetime, while the energy-dependent term, $\Gamma_{\text{mfp}}(E)$, represents all of the intrinsic and extrinsic inelastic processes. The $\Gamma_{\text{mfp}}(E)$ function is zero below an onset energy, E_s (which in extended systems corresponds to the plasmon excitation energy), and begins to increase from a value A_s, following the universal functional form of the mean free path in solids. In all analyses, the Γ_c value was fixed to 1.55 eV. Both the onset energy E_s and the jump A_s are introduced in the $\Gamma_{\text{tot}}(E)$ function via an arctangent functional to avoid discontinuities and to simulate the electron−hole pair excitations. Their numerical values are derived at each computational step (i.e., for each geometric configuration) on the basis of a Monte Carlo fit. The experimental resolution is taken into account by a Gaussian convolution.

The minimization of the MeOH XANES spectrum has been carried out starting from the X-ray structure of hexamethanoloiron diiodide,[40] substituting the Cu atom and different MeOH molecules to test possible coordination geometries. During minimization, the relative orientation of the methyl groups has been kept fixed, with a Cu−O−C angle of 129.5°, which is the value of the Fe−O−C angle in the hexamethanoloiron diiodide X-ray structure. In the case of the DMSO solution, hexakis(dimethyl sulfoxide)copper(II) bis(hydrogen sulfate) has been used as the starting model.[41] In this case, different possible complexes have been tested and the Cu−O distances and O−Cu−O angle have been minimized. The H atoms have been included in all MXAN analyses.

Least-square fits of the experimental data in the space of the structural parameters were achieved by minimizing the residual function defined as

$$R_{\text{sq}} = \frac{\sum_{i=1}^{m} w_i(y_i^{\text{th}} - y_i^{\text{exp}})^2}{\varepsilon_i^2 \sum_{i=1}^{m} w_i} \quad (2)$$

where m is the number of data points, y_i^{th} and y_i^{exp} are the theoretical and experimental values of absorption, respectively, ε_i is the individual error in the experimental data set, and w_i is a statistical weight. For $w_i = $ constant $= 1$, the square residual function, R_{sq}, becomes the statistical χ^2 function. Here, we assumed a constant experimental error, $\varepsilon = 1.2\%$, for the whole experimental data set. Five nonstructural parameters
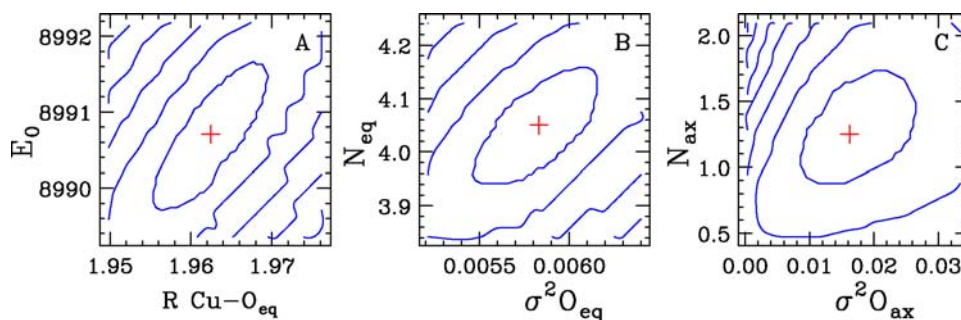
Figure 1. Two-dimensional contour plots for selected parameters in the EXAFS fit of the Cu K-edge spectrum of Cu^{2+} in a MeOH solution: (A) $Cu-O_{eq}$ distance versus E_0; (B) $Cu-O_{eq}$ coordination number versus DW factor; (C) $Cu-O_{ax}$ coordination number versus DW factor.
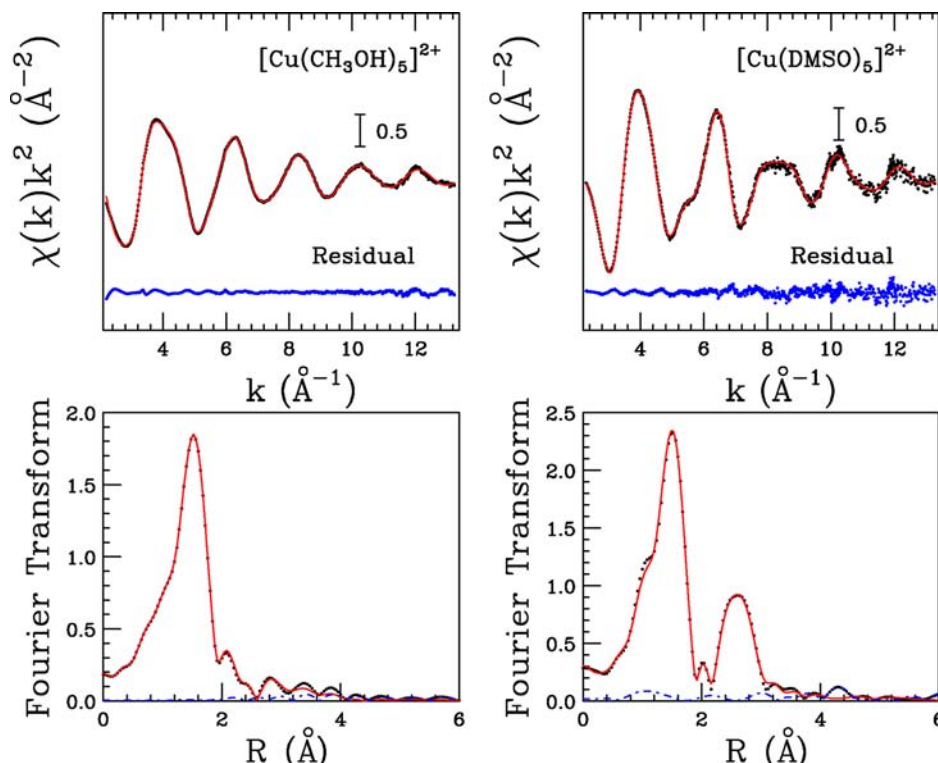

Figure 2. Comparison of the experimental Cu K-edge EXAFS spectra of Cu^{2+} in MeOH and DMSO solutions (red, solid line) and the theoretical signals calculated for a 5-fold square-pyramidal geometry (black, dotted line). In the lower panels, comparisons of the modulus of the FT of the experimental k^2-weighted EXAFS spectra (red, solid line) and the fitting results (black, dotted line) are shown.

have been optimized, namely, the Fermi energy level E_F, the experimental resolution Γ_{exp}, the threshold energy E_0, and the energy and amplitude of the plasmon, E_s and A_s.

3. RESULTS

3.1. EXAFS Analysis. In the first step, the EXAFS spectra have been analyzed using a variable number of ligands in the equatorial plane and in the axial positions. From this analysis, it was possible to assess the sensitivity of EXAFS toward the coordination numbers and distances. In particular, to establish error limits in the refined parameters, a statistical analysis applying two-dimensional contour plots to selected parameters of the fit was applied. This analysis examines the correlations among fitting parameters and evaluates the statistical errors by following the procedure described in detail in ref 33. Figure 1 shows, as an example, the contour plots of the $Cu-O_{eq}$ distance versus E_0 for the MeOH solution, together with the $Cu-O_{eq}$ and $Cu-O_{ax}$ coordination numbers and Debye–Waller (DW) factors, where the innermost contour refers to the 95% error

confidence interval. From this figure, it is evident that the $Cu-O_{eq}$ distances can be determined from EXAFS analysis with high accuracy. In the case of the equatorial ligands, the correlation between the coordination number and DW factor is much smaller compared to that of the axial ligands. As a consequence, the error in the determination of the number of MeOH molecules bound to the Cu^{2+} ion in the equatorial plane is much smaller compared to that of the axial ligands and, therefore, the EXAFS technique alone is not able to determine the number of axial coordinating ligands with sufficient accuracy. The same analysis was also carried out for the DMSO solution, giving similar results.

Therefore, for both systems, EXAFS analysis was carried out assuming the presence of four ligands in the equatorial plane and either one or two axial ligands, representing a square-pyramidal or a JT distorted octahedral configuration, respectively. The best-fit analyses of the MeOH and DMSO EXAFS spectra are shown in Figure 2 for the 5-fold
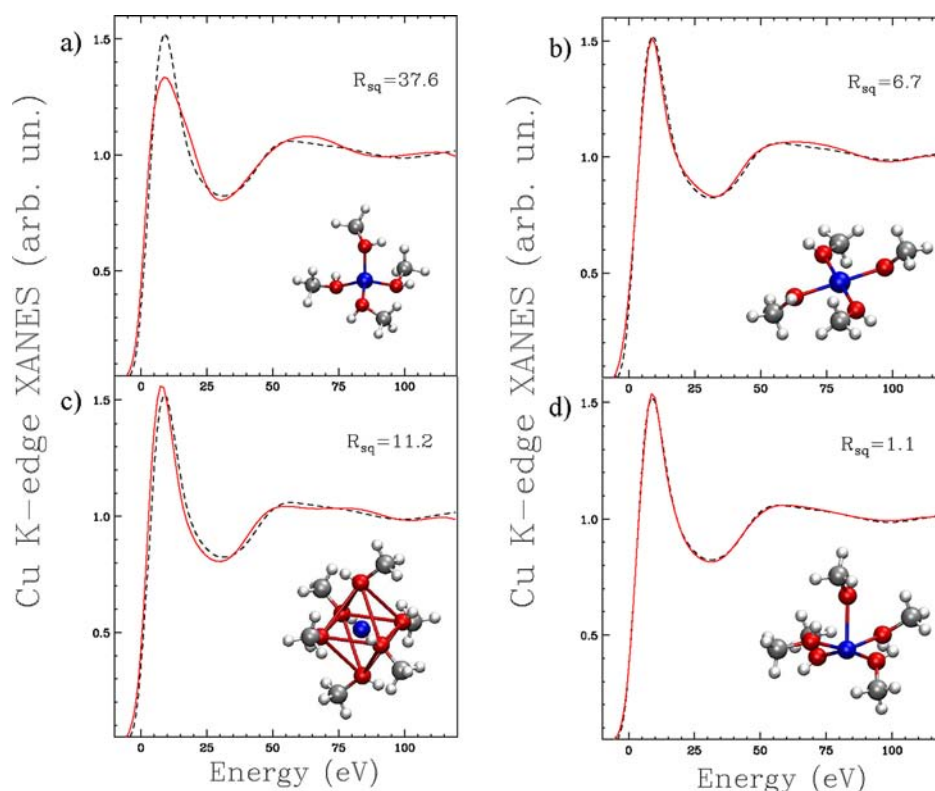
Figure 3. Comparison of the Cu K-edge XANES experimental spectrum of Cu^{2+} in a MeOH solution (black, dashed line) and the theoretical spectra (red, full line) calculated with a regular tetrahedral model (a), with a square-planar model (b), with an axially elongated octahedral model (c), and with an elongated square-pyramidal model (d).

coordination model and in Figure S1 in the Supporting Information (SI) for the 6-fold coordination model. During these fitting procedures, the coordination numbers and the MeOH and DMSO geometries have been kept fixed. The upper panels of Figure 2 show the total $\chi(k)$ theoretical signals associated with a 5-fold pyramidal geometry of the ligands around the Cu^{2+} ion, compared with the experimental spectra, and the resulting residuals. The $\chi(k)$ signals are shown multiplied by k^2 for a better visualization. In analysis of the MeOH solution, the following contributions have been included: the $Cu-O_{eq}$, $Cu-O_{ax}$ and $Cu-H_{eq}$ two-body signals and the $Cu-O_{eq}-C_{eq}$ and $O_{eq}-Cu-O_{eq}$ three-body signals, as shown in Figure S2 in the SI. All of the signals used for DMSO are shown in Figure S3 in the SI. The lower panels of Figure 2 show the corresponding k^2-weighted Fourier transform (FT) calculated with no phase-shift correction applied, in the k range of 2.8–13.0 Å^{-1}. Simple inspection of the FT spectra offers interesting insight into the structural information that can be obtained from the EXAFS technique. In the left lower panels of Figures 2 and S1 in the SI, the peak at about 1.5 Å is associated with the Cu−O and Cu−H MeOH first-shell contributions. In this case, the methyl C atoms provide a small contribution at about 2.2 Å. In the case of Cu^{2+} in a DMSO solution (right lower panels of Figures 2 and S2 in the SI), the main peak at about 1.5 Å is associated with the Cu−O first-shell distance and the second peak at about 2.6 Å is essentially due to the Cu−O−S MS signal and to the Cu···S two-body contribution. The outstanding result of these analyses is that the EXAFS experimental data of the MeOH and DMSO solutions can be reproduced with the same accuracy using both a square-pyramidal or a JT distorted octahedral coordination. The R_i values obtained from the minimizations are 6.5×10^{-6} and 6.7

$\times 10^{-6}$ for the 5- and 6-fold coordination in a MeOH solution, respectively, and 1.6×10^{-5} and 1.7×10^{-5} for the 5- and 6-fold coordination in a DMSO solution, respectively. The structural parameters obtained from the fitting procedures are reported in Table 1. For both solvents, the Cu−O equatorial and axial distances are in good agreement with the values previously determined in water[3,5] and in different organic solvents.[13,14] As far as the Cu−O axial distances are concerned, a small shortening and a decrease of the DW factors are obtained when a 5-fold geometry is considered in the fitting procedure. As a result, while the structural determination is very accurate as far as the shell distances are concerned, EXAFS analysis is inconclusive regarding the different coordination polyhedra of the solvent structure of Cu^{2+} ion in the two solvents. This result is not surprising considering the large error in the determination of the axial coordination number that was evidenced by the correlation maps reported in Figure 1.

3.2. XANES Analysis. To get a deeper insight into the geometry of the complexes that the Cu^{2+} ion forms in MeOH and DMSO, we resorted to the use of XANES, which is extremely sensitive to the geometric environment of the absorbing atom because it takes specific account of the XAS edge region where MS effects make large contributions to XAS spectra.

3.2.1. Cu^{2+} in a MeOH Solution. In the first step of analysis, the compatibility of the XANES spectrum with the existence of four-coordinated complexes in MeOH was assessed by performing a minimization of the experimental data while imposing a tetrahedral or square-planar geometry. In these fits, only the Cu−MeOH ligand distances were allowed to vary, while the relative orientation of the methyl groups has been kept fixed, with a Cu−O−C angle of 129.5°, which is the value

of the Fe−O−C angle in the hexamethanoloiron diiodide X-ray structure, which was taken as the starting model for the minimization procedure.[40] The results of the fitting procedures are shown in parts a and b of Figure 3 and correspond to an ideal tetrahedral configuration with four O atoms at 1.99 Å and a square-planar geometry with four O atoms at 2.00 Å, respectively (see Table 2). The agreement between the

Table 2. Cu K-edge XANES Structural Parameters of Cu^{2+} in MeOH and DMSO Solutions^{a}

	Cu−O$_{eq1}$(Å)	Cu−O$_{eq2}$(Å)	Cu−O$_{ax}$(Å)	R$_{sq}$
Cu^{2+} in MeOH				
4-fold tetrahedral	1.99(2)	1.99(2)	-	37.6
4-fold square planar	2.00(2)	2.00(2)	-	6.7
5-fold	1.95(2)	2.01(2)	2.23(5)	1.1
6-fold	1.95(2)	1.95(2)	2.23(4)	11.2
Cu^{2+} in DMSO				
4-fold tetrahedral	2.02(2)	2.02(2)	-	19.7
4-fold square planar	2.01(2)	2.01(2)	-	4.1
5-fold	1.97(2)	1.97(2)	2.23(4)	1.2
6-fold	1.95(2)	1.95(2)	2.23(4)	9.7

^{a}Cu−O$_{eq1}$ and Cu−O$_{eq2}$ are the distances between the ion and the equatorial O atoms; Cu−O$_{ax}$ is the distance between the ion and the axial O atoms; R$_{sq}$ is the residual function.

experimental curve and the calculated model shown in Figure 3a is quite poor, and this is also evident from the high value of the residual function, R$_{sq}$ = 37.6, while a square-planar structure (Figure 3b) better reproduces the experimental data (R$_{sq}$ = 6.7).

In the second step, the compatibility of the XANES data with a JT distorted 6-fold octahedral model was tested while allowing all of the Cu−MeOH distances to vary. The results of this analysis are shown in Figure 3c. The agreement between the experimental data and the best-fit calculation is not very good, displaying a mismatch in the entire energy region. The values of the best-fit structural parameters correspond to a JT distorted octahedron geometry, with four O atoms at 1.95 Å and two axial O atoms at 2.23 Å (see Table 2). An additional fit was carried out, allowing the O$_{ax}$−Cu−O$_{eq}$ angles to vary, but the best-fit model retained a JT distorted octahedral geometry.

The geometrical arrangement that best reproduces the experimental data was obtained by performing XANES analysis starting from a five-coordinate square pyramid and allowing the

four equatorial ligands to leave the equatorial plane, in addition to allowing all of the Cu−MeOH distances to vary. The results of the minimization are depicted in Figure 3d. This new fit shows a very good agreement between the experimental and theoretical spectra (R$_{sq}$ = 1.1), and it corresponds to an elongated square-pyramidal geometry with the axial O atoms at 2.23 Å, two ligands distorted by 11 ± 4° from the equatorial plane at 2.01 Å, and two ligands distorted by 14 ± 4° from the equatorial plane at 1.95 Å. Figure 4 displays the structural model obtained from this fit, while the corresponding structural parameters are reported in Table 2. Finally, a trigonal-bipyramidal model with three equatorial and two axial ligands has been used to fit the XANES data, and the results are shown in Figure S4 in the SI. Given the poor agreement between the experimental and theoretical spectra, this model can be discarded. The structural parameters obtained from XANES analysis for the elongated square-pyramidal complex are in good agreement with the EXAFS results within the statistical errors. The very good reproduction of the experimental data and the agreement between the EXAFS and XANES determinations of the first-shell bond lengths suggest that the five-coordinate square-pyramidal complex is the predominant species present in a MeOH solution.

3.2.2. Cu^{2+} in DMSO Solution. In the case of the DMSO solution, the XANES spectrum has been analyzed along the line of the previous investigation and different solvation complexes have been used as starting models. All of the fits have been performed, allowing only the Cu−DMSO first-shell distance to vary and keeping the S−O distance and Cu−O−S angle fixed to the values of the crystal structure of hexakis(dimethyl sulfoxide)copper(II) bis(hydrogen sulfate), which was used as the starting model in the minimization procedure.[41] In this solid-state crystal, the Cu^{2+} ion coordinates six DMSO ligands in a JT distorted octahedral configuration with two axial O atoms at 2.34 Å, two equatorial O atoms at 1.98 Å, and two equatorial O atoms at 2.02 Å.

The first coordination scheme considered a 4-fold geometry around the Cu^{2+} ion having either a tetrahedral or a square-planar configuration. During the minimization, two different sets of distances were considered, but a regular geometry was detected in both cases, with a Cu−O distance of 2.02 (2.01) Å. The best-fit results of these analyses are shown in Figure 5a,b, for the tetrahedral and square-planar structures, respectively. The structural parameters are listed in Table 2. As was previously found for the MeOH solution, use of a 4-fold
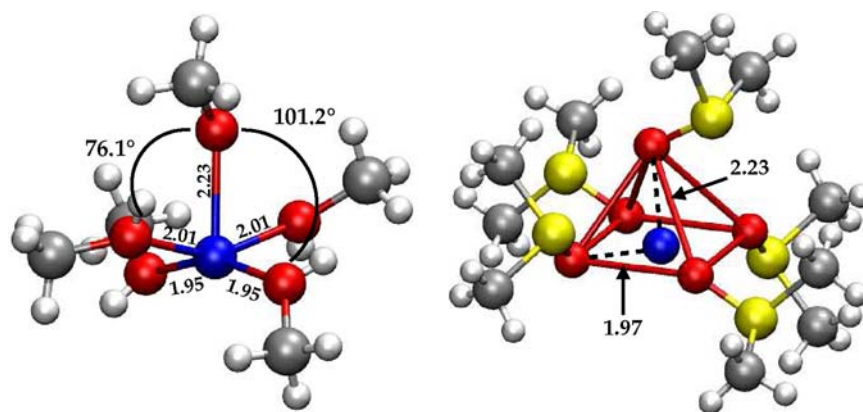

Figure 4. Structural representation of the best-fit 5-fold-elongated square-pyramidal model for Cu^{2+} in a MeOH solution (left side) and in a DMSO solution (right side).
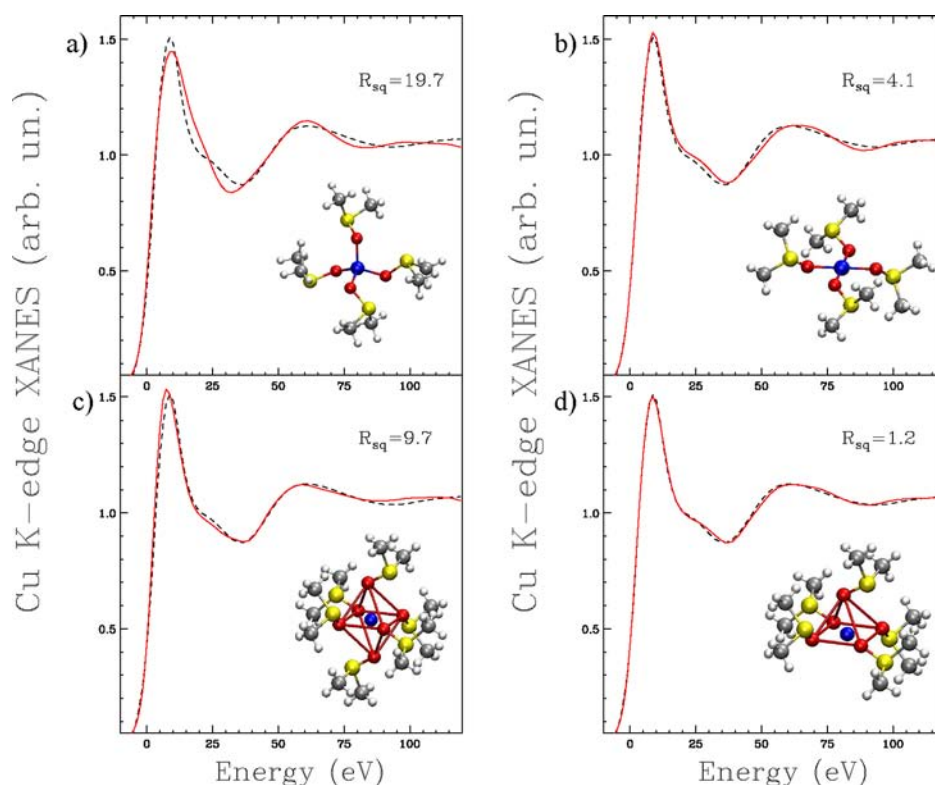
Figure 5. Comparison of the Cu K-edge XANES experimental spectrum of Cu^{2+} in a DMSO solution (black, dashed line) and the theoretical spectra (red, full line) calculated with a regular tetrahedral model (a), with a square-planar model (b), with an axially elongated octahedral model (c), and with an elongated square-pyramidal model (d).

coordination provides theoretical spectra that are not in perfect agreement with the experimental data, and this is testified by the rather high error index values (see Table 2). In particular, the tetrahedral geometry gives rise to a XANES spectrum lacking the main features present in the experimental data.

In the second step, we have considered a Cu^{2+} environment in which six DMSO molecules surround the metal, forming a JT distorted octahedron, similar to the environment found in the copper DMSO solvate solid sulfate. The best-fit results of this analysis are shown in Figure 5c, but the agreement of the computed spectrum with the experimental data is not perfect. Also in this case, an additional fit was carried out, allowing the $O_{ax}-Cu-O_{eq}$ angles to vary, but the best-fit model retained a JT distorted octahedral geometry.

As shown in Figure 5d, the closest match to the experimental spectrum is obtained using a square-pyramidal 5-fold coordination model with the axial O atom at 2.23 Å and four O atoms in the equatorial plane at 1.97 Å. Also in this case, we allowed the four equatorial ligands to leave the equatorial plane, but in DMSO, there is no ligand displacement from the mean equatorial plane, probably because of the steric hindrance of the ligands. The structural model resulting from this fit is shown in Figure 4 and is similar to the one of Cu^{2+} in a MeOH solution, while the refined structural parameters are summarized in Table 2 and are in good agreement, within the statistical errors, with the EXAFS and crystallographic determinations.

4. DISCUSSION AND CONCLUSIONS

In this work, we have studied the solvation structure of the Cu^{2+} ion in MeOH and DMSO solutions, by combining the EXAFS and XANES techniques. The EXAFS analysis is not conclusive regarding the coordination geometry of the MeOH-

and DMSO-solvated complexes. Therefore, we have carried out a quantitative analysis of the Cu K-edge XANES spectra, testing several possible coordination environments. In particular, the XANES analysis has revealed the existence of a 5-fold square-pyramidal complex in both the MeOH and DMSO solutions, in contrast with the usual JT distorted geometry previously found. This result is not surprising because the Cu^{2+} ion has recently been found to have a similar 5-fold coordination also in water. In particular, on the basis of a combination of the neutron diffraction and molecular dynamics data, it was determined that the Cu^{2+} ion coordinates five water molecules. The calculations have shown that the aqua complex of the ion experiences frequent conversions between configurations of a square pyramid and a trigonal bipyramid.[2] More recent studies combining XANES and EXAFS methods have confirmed the coordination of five water molecules by the Cu^{2+} ion, and a distortion of the regular square-pyramidal configuration has been found.[3,5] Such a conclusion was confirmed by molecular dynamics and density functional theory studies, where it was found that the Cu^{2+} ion coordinates four water molecules in the equatorial position at a distance of 2.00 Å and one water molecule in the axial position at a distance of 2.45 Å.[42,43]

To better rationalize the behavior of Cu^{2+} in MeOH and DMSO solutions, it is important to note that the bonds of the ion with the equatorial O atoms have the covalent nature, whereas the interaction with the O atoms in the axial positions has only the electrostatic nature.[42] As a result, the axial ligand bonds are weaker compared to the equatorial ones, and the solvent molecules in the axial positions undergo a fast exchange with the bulk solvent. It is important to stress that X-ray structural analysis detects the so-called diffusion-averaged structure, i.e., the structure averaged with respect to the

whole time of the experiment, whereas the calculation methods detect structures realized within shorter time intervals. Therefore, our results and the determined geometry of the complexes suggest a dynamical picture in which the axial ligands undergo a fast exchange with the second-shell solvent molecules, giving rise to a mean axial coordination number equal to 1. Note that several 5-fold-coordinated Cu^{2+} ions are present in crystalline compounds, suggesting that these coordinations are competitive.[44] Moreover, also the Cu^{2+} aqua ion has been found to adopt a 5-fold coordination.[2,3,5] This is a direct consequence of the $3d^9$ electronic structure of its atomic shell, which causes a departure from octahedral coordination because of the JT effect. The present experimental results can stimulate deeper theoretical and experimental investigations of the solvation environment and dynamics of the Cu^{2+} ion in nonaqueous solutions.

■ ASSOCIATED CONTENT

Ⓢ Supporting Information

Figures S1–S4. This material is available free of charge via the Internet at http://pubs.acs.org.

■ AUTHOR INFORMATION

Corresponding Author

*E-mail: p.dangelo@caspur.it (P.D.), zitolo@caspur.it (A.Z.).

Notes

The authors declare no competing financial interest.

■ ACKNOWLEDGMENTS

■ REFERENCES

(1) Ohtaki, H.; Radnai, T. *Chem. Rev.* **1993**, *93*, 1157–1204.

(2) Pasquarello, A.; Petri, I.; Salmon, P. S.; Parisel, O.; Car, R.; Toth, E.; Powell, D. H.; Fischer, H. E.; Helm, L.; Merbach, A. *Science* **2001**, *291*, 856–859.

(3) D'Angelo, P.; Benfatto, M.; Della Longa, S.; Pavel, N. V. *Phys. Rev. B* **2002**, *66*, 064209–7.

(4) Blumberger, J.; Bernasconi, L.; Tavernelli, I.; Vuilleumier, R.; Sprik, M. *J. Am. Chem. Soc.* **2004**, *126*, 3928–3938.

(5) Frank, P.; Benfatto, M.; Szilagyi, R. K.; D'Angelo, P.; Della Longa, S.; Hodgson, K. O. *Inorg. Chem.* **2005**, *44*, 1922–1933.

(6) Xia, F. F.; Yi, H.-B.; Zeng, D. *J. Phys. Chem. A* **2010**, *114*, 8406–8416.

(7) Liu, X.; Lu, X.; Meijer, E. J.; Wang, R. *Phys. Chem. Chem. Phys.* **2010**, *12*, 10801–10804.

(8) Frank, P.; Benfatto, M.; Hedman, B.; Hodgson, K. O. *Inorg. Chem.* **2008**, *47*, 4126–4139.

(9) Frank, P.; Benfatto, M.; Hedman, B.; Hodgson, K. O. *Inorg. Chem.* **2012**, *51*, 2086–2096.

(10) Inada, Y.; Sugimoto, K.; Ozutsumi, K.; Funahashi, S. *Inorg. Chem.* **1994**, *33*, 1875–1880.

(11) Ozutsumi, K.; Abe, Y.; Takahashi, R.; Ishiguro, S. *J. Phys. Chem.* **1994**, *98*, 9894–9899.

(12) Ozutsumi, K.; Koide, M.; Suzuki, H.; Ishiguro, S. *J. Phys. Chem.* **1993**, *97*, 500–502.

(13) Inada, Y.; Hayashi, H.; Sugimoto, K.; Funahashi, S. *J. Phys. Chem. A* **1999**, *103*, 1401–1406.

(14) Persson, I.; Penner-Hahn, J. E.; Hodgson, K. O. *Inorg. Chem.* **1993**, *32*, 2497–2501.

(15) Helm, L.; Lincoln, S. F.; Merbach, A. E.; Zbinden, D. *Inorg. Chem.* **1986**, *25*, 2550–2552.

(16) Magini, M. *Inorg. Chem.* **1982**, *21*, 1535–1538.

(17) Licheri, G.; Musinu, A.; Paschina, G.; Piccaluga, G.; Pinna, G.; Sedda, A. F. *J. Chem. Phys.* **1984**, *80*, 5308–5311.

(18) Beagley, B.; Eriksson, A.; Lindgren, J.; Persson, I.; Pettersson, L. G. M.; Sandstrom, M.; Wahlgren, U.; White, E. W. *J. Phys.: Condens. Matter* **1989**, *1*, 2395–2408.

(19) Salmon, P. S.; Neilson, G. W. *J. Phys.: Condens. Matter* **1989**, *1*, 5291–5295.

(20) D'Angelo, P.; Bottari, E.; Festa, M. R.; Nolting, H. F.; Pavel, N. V. *J. Chem. Phys.* **1997**, *107*, 2807–2812.

(21) D'Angelo, P.; Di Nola, A.; Mangoni, M.; Pavel, N. V. *J. Chem. Phys.* **1996**, *104*, 1779–1790.

(22) Chillemi, G.; Mancini, G.; Sanna, N.; Barone, V.; Della Longa, S.; Benfatto, M.; Pavel, N. V.; D'Angelo, P. *J. Am. Chem. Soc.* **2007**, *129*, 5430–5436.

(23) D'Angelo, P.; Bottari, E.; Festa, M. R.; Nolting, H. F.; Pavel, N. V. *J. Phys. Chem. B* **1998**, *102*, 3114–3122.

(24) Roccatano, D.; Berendsen, H. J. C.; D'Angelo, P. *J. Chem. Phys.* **1998**, *108*, 9487–9497.

(25) D'Angelo, P.; De Panfilis, S.; Filipponi, A.; Persson, I. *Chem.— Eur. J.* **2008**, *14*, 3045–3055.

(26) D'Angelo, P.; Pavel, N. V. *J. Chem. Phys.* **1999**, *111*, 5107–5115.

(27) Chillemi, G.; Barone, V.; D'Angelo, P.; Mancini, G.; Persson, I.; Sanna, N. *J. Phys. Chem. B* **2005**, *109*, 9186–9193.

(28) D'Angelo, P.; Chillemi, G.; Barone, V.; Mancini, G.; Sanna, N.; Persson, I. *J. Phys. Chem. B* **2005**, *109*, 9178–9185.

(29) D'Angelo, P.; Persson, I. *Inorg. Chem.* **2004**, *111*, 3543–3549.

(30) Zitolo, A.; D'Angelo, P. *Chem. Phys. Lett.* **2010**, *499*, 113–116.

(31) Migliorati, V.; Chillemi, G.; D'Angelo, P. *Inorg. Chem.* **2011**, *50*, 8509–8515.

(32) Hayakawa, K.; Hatada, K.; D'Angelo, P.; Della Longa, S.; Natoli, C. R.; Benfatto, M. *J. Am. Chem. Soc.* **2004**, *126*, 15618–15623.

(33) Filipponi, A.; Di Cicco, A. *Phys. Rev. B* **1995**, *52*, 15135–15149.

(34) Filipponi, A.; Di Cicco, A.; Natoli, C. R. *Phys. Rev. B* **1995**, *52*, 15122–15134.

(35) Benfatto, M.; Della Longa, S. *J. Synchrotron Radiat.* **2001**, *8*, 1087–1094.

(36) Benfatto, M.; Della Longa, S.; Natoli, C. R. *J. Synchrotron Radiat.* **2003**, *10*, 51–57.

(37) Della Longa, S.; Arcovito, A.; Girasole, M.; Hazemann, J. L.; Benfatto, M. *Phys. Rev. Lett.* **2001**, *87*, 155501–155504.

(38) Hermes, C.; Gilberg, E.; Koch, M. *Nucl. Instrum. Methods Phys. Res.* **1984**, *222*, 207–214.

(39) Pettifer, R. F.; Hermes, C. *J. Appl. Crystallogr.* **1985**, *18*, 404–412.

(40) Harms, K.; Biesemeier, F.; Mueller, U. *Z. Kristallogr., New Chem. Sci.* **2003**, *218*, 164–164.

(41) Bieller, S.; Lerner, H. W.; Bolte, M. *Acta Crystallogr., Sect. E* **2005**, *61*, m928–m929.

(42) Amira, S.; Spangberg, D.; Hermansson, K. *Phys. Chem. Chem. Phys.* **2005**, *7*, 2874–2880.

(43) Bryantsev, V. S.; Diallo, M. S.; van Duin, A. C.; Goddard, W. A., III. *J. Phys. Chem. A* **2008**, *112*, 9104–9112.

(44) Hathaway, B. J. In *Comprehensive Coordination Chemistry*; Wilkinson, G., Ed.; Pergamon: Oxford, U.K., 1987; Vol. 5, pp 533–774.